itle

subtitleubtitle

subjectubject

uthor

Delft University of Technology

TU Delft

List of Figures

List of Tables

Contents

Chapter 1

Orbital Mechanics

At the core of astrodynamics, the two-body restricted problem describes the motion of a secondary body of negligible mass orbiting a central body, with no other sources of acceleration in the system. This problem is described by Newton's equation of planetary motion

$$\ddot{\mathbf{r}} = -\frac{\mu}{r^3}\mathbf{r}, \tag{1.1}$$

where $\mathbf{r}$ = the Cartesian, a.k.a. the rectangular coordinate position vector relative to the central body,

$\mu = GM$ = the gravitational parameter of the central body,

G = the universal gravitational constant,

M = the mass of the central body.

1.1. 1Reference Frames

There are various categories of reference frames used within astrophysics and astrodynamics. Some frames are *outdated* in nature, but are however still documented and commonly used to ensure the usability of historical empirical data. This section will cover the generalised taxonomy of these reference frames, with mention of common frames and where they fit within the taxonomy.

Unless stated otherwise, one should assume that all orthogonal reference frames used within astrodynamics are right handed, defined by $\mathbf{X} \times \mathbf{Y} = \mathbf{Z}$ as illustrated in Figure 1.1. The contemporary reference systems used in astronomy and astrophysics are defined International Astronomical Union (IAU). Due to the long history of the field, there are many others outside of the IAU's standardised frames which are still used for a multitude of reasons, one being the need to ensure accessibility to older observations

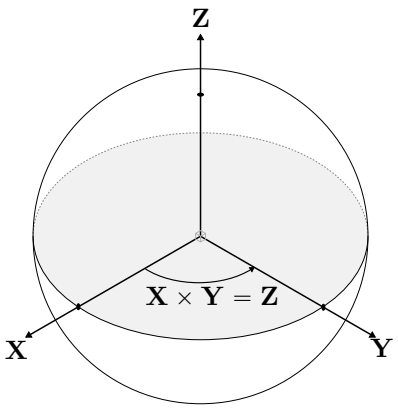

Figure 1.1: Definition of a right-handed reference frame.

which were made in the older alternative systems.

A. 1Earth-centred inertial (ECI)

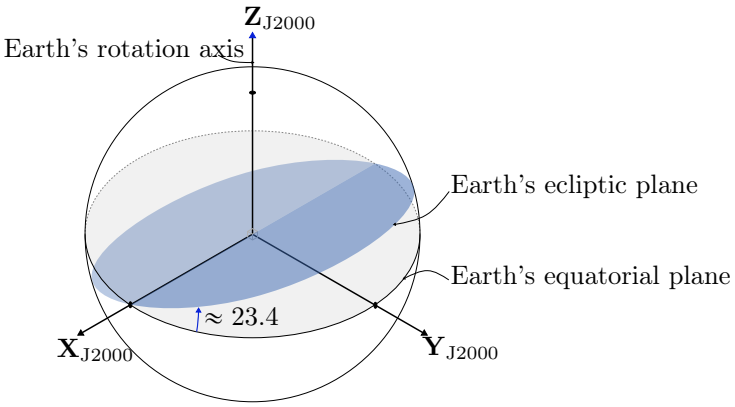

Figure 1.2: Definition of the J2000 Earth-centred inertial (ECI) frame.

B. 1Inertial

An inertial reference frame is a non-rotating frame with a non-accelerating origin. All inertial reference frames are in a state of constant rectilinear motion with respect to one another. Strictly speaking, "inertial" is used in place of "quasi-inertial", as no reference frame we use is truly non-accelerating. This approximation is accepted due to the near negligible acceleration these frames' origins. From this point forwards, "inertial" will be used in place of "quasi-inertial". There are two frames which are used in astrophysics as the lowest level in the hierarchy, namely J2000 (a.k.a. EME2000) and the International Celestial Reference Frame (ICRF).

Include illustrations for the J2000 (EMEJ2000) frame and the origin of its definition. Explain how ICRS was an interaction on this frame. Explain also how J2000 is related to the Earth-centered inertial (ECI) reference frame, leading to the next subsection on BCI.

C. 1Body-centered inertial (BCI)

The Body-centered inertial (BCI) reference frames are frames which have their origins at the center of mass of a body, the Z_C-axis is directed along the (counter clockwise positive) spin-axis of the body, the X_C-axis passes through the ascending node of the intersection between the ecliptic and the equator of the body. The Y_C-axis then passes through the equatorial plane perpendicular to X_C and Z_C-axis to complete the rectangular coordinate system.

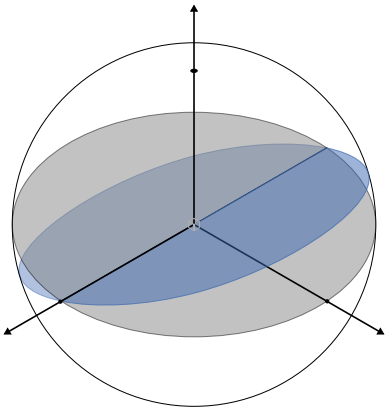

Figure 1.3: Definition of a general Body-centered inertial (BCI) reference frame.

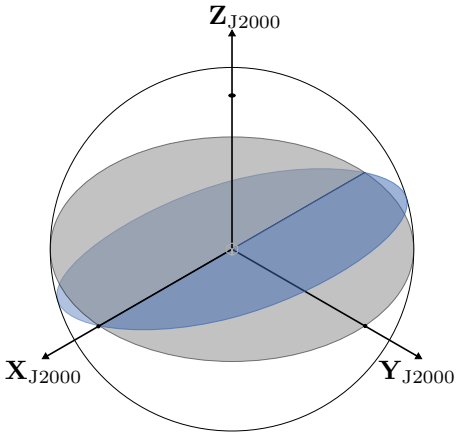

Figure 1.4: Definition of a general Body-centered inertial (BCI) reference frame.

D. 1Body-centered body-fixed (BCBF)

The body-centered body-fixed (BCBF) reference frames are frames which have their origins at the center of mass of a body, the Z_F-axis is directed along (counter clockwise positive) spin-axis of the body. The X_F-axis passes through the reference meridian of the body, which is at an angle of $\Omega_t t_0$ from the ascending node of the intersection between the ecliptic and the equator of the body. The Y_F-axis then passes through the equatorial plane perpendicular to X_F and Z_F.

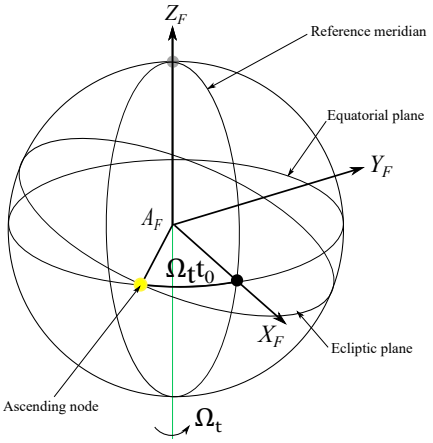

Figure 1.5: Definition of a general Body-centered body-fixed (BCBF) reference frame.

$$W = W_0 + \dot{W}d \tag{1.2}$$

where, W = the ephemeris position of the prime meridian

W_0 = the value of W at J2000.0 (occasionally some other epoch),

d = interval in days from the standard epoch.

$$\mathbf{R}^{I/B} = \mathbf{R}_z(W)\mathbf{R}_x(\pi/2 - \delta_0)\mathbf{R}_z(\pi/2 - \alpha_0) \tag{1.3}$$

where, $\mathbf{R}_{x,y,z}(\phi)$ = transformation matrix for a rotation of ϕ radians about the respective axis (subsection 4.3.5),

α_0, δ_0 = ICRF equatorial coordinates at epoch J2000.0

E. 1Radial tangential normal (RTN)

The radial tangential normal frame (RTN), a.k.a. the radial (R), along-track (S) and cross-track (W) frame (RSW), is a dynamic frame with an orbiting spacecraft at the centre of the frame. The frame is time dependent and based on the two-body restricted problem problem with the R-component determined by the current unit-vector of position $\hat{r}$, the T-component by the unit vector of velocity $\hat{v}$, and the N-component by their the cross product of the two, the specific angular momentum vector $\hat{r} \times \hat{v} = \hat{h}$. This frame is commonly used for relative motion of spacecraft in a rendezvous segment.

$$\mathbf{R}^{I/RSW} = \left[\hat{\mathbf{r}}_{B/S}\ \hat{\mathbf{v}}_{B/S}\ \hat{\mathbf{h}}_{B/S}\right] \tag{1.4}$$

where, $\hat{\mathbf{r}}_{B/S}$ = the position of the spacecraft with respect to the body,

$\hat{\mathbf{v}}_{B/S}$ = the velocity of the spacecraft with respect to the body,

$\hat{\mathbf{h}}_{B/S}$ = the specific angular momentum of the spacecraft with respect to the body,

1.2. 1Orbital Elements

Orbital elements are a set of parameters which uniquely define a Keplerian, or two-body restricted orbit, around a given central body in the absence of any external perturbations incurred in the system. This definition is given with with respect to a plane of reference and a reference direction. Conversion between any arbitrary pair of orbital elements of a given reference plane and direction, requires only the central body's gravitational parameter μ.

A. 1Cartesian

The Cartesian, a.k.a. the rectangular orbital elements are the concatenation of the position and velocity vectors in the respectively named coordinate system relative to the central body,

$$\mathfrak{E}_C = \begin{bmatrix} \mathbf{r}^T & \mathbf{v}^T \end{bmatrix}^T = \begin{bmatrix} r_x & r_y & r_z & v_x & v_y & v_z \end{bmatrix}^T, \tag{1.5}$$

where all values are assumed as S.I. units, where not specified otherwise, in further calculations involving the orbital elements.

B. 1Keplerian

The Keplerian, a.k.a. the classical orbital elements are the

$$\mathfrak{E}_K = \begin{bmatrix} a & e & i & \Omega & \omega & \theta \end{bmatrix}^T, \tag{1.6}$$

C. 1Modified Equinoctial

The Keplerian, a.k.a. the classical orbital elements are the

$$\mathfrak{E}_{ME} = \begin{bmatrix} p & f & g & h & k & L \end{bmatrix}^T, \tag{1.7}$$

$$\begin{aligned} p =& a(1-e^2) \\ f =& e\cos(\omega+\Omega) \\ g =& e\cos(\omega+\Omega) \\ h =& \tan(i/2)\cos\Omega \\ k =& \tan(i/2)\sin\Omega \\ L =& \Omega+\omega+\theta \end{aligned} \tag{1.8}$$

[?]

1.3. 1Preliminary Orbit Determination

A. 1Gibbs method

B. 1Lambert's problem

C. 1Gauss method

1.4. 1Orbital Perturbations

In order to account for perturbations such as a non-spherical body, atmospheric drag, propulsive thrust, solar radiation pressure, and other celestial objects outside the two-body formulation, Equation 1.1 can be rewritten as

$$\ddot{\mathbf{r}} = \frac{\mu}{|\mathbf{r}|^3}\mathbf{r} + \mathbf{p}, \tag{1.9}$$

where $\mathbf{p}$ is the net perturbative accelerations from all sources other than the spherically symmetric gravitational attraction between the two bodies.

A. 1Cowell's method

$$\ddot{\mathbf{r}} = \frac{\mathrm{d}\dot{\mathbf{r}}}{\mathrm{d}t} = -\frac{\mu}{r^3}\mathbf{r} + \mathbf{p} \tag{1.10}$$

B. 1Encke's method

C. 1Variational Equations: Lagrange Planetary

$$
\begin{aligned}
\frac{\mathrm{d}a}{\mathrm{d}t} &= -\frac{2a^2}{\mu}\frac{\partial R}{\partial t_p} \\
\frac{\mathrm{d}e}{\mathrm{d}t} &= -\frac{\sqrt{1-e^2}}{\sqrt{\mu a}e}\frac{\partial R}{\partial a} + \frac{a(1-e^2)}{\mu e}\frac{\partial R}{\partial t_p} \\
\frac{\mathrm{d}t_p}{\mathrm{d}t} &= \frac{2a^2}{\mu}\frac{\partial R}{\partial a} + \frac{a(1-e^2)}{\mu e}\frac{\partial R}{\partial e} \\
\frac{\mathrm{d}\Omega}{\mathrm{d}t} &= \frac{1}{\sqrt{\mu a(1-e^2)}\sin i}\frac{\partial R}{\partial i} \\
\frac{\mathrm{d}i}{\mathrm{d}t} &= \frac{1}{\sqrt{\mu a(1-e^2)}}\left(\frac{1}{\tan i}\frac{\partial R}{\partial \omega} - \frac{1}{\sin i}\frac{\partial R}{\partial \Omega}\right) \\
\frac{\mathrm{d}\omega}{\mathrm{d}t} &= -\frac{1}{\sqrt{\mu a(1-e^2)}\tan i}\frac{\partial R}{\partial i} + \frac{\sqrt{1-e^2}}{\sqrt{\mu a}e}\frac{\partial R}{\partial e}
\end{aligned}
\tag{1.11}
$$

D. 1Variational Equations: Gauss

$$
\begin{aligned}
\frac{\mathrm{d}a}{\mathrm{d}t} &= 2\sqrt{\frac{a}{\mu}}\left(F_R\frac{ae}{\sqrt{1-e^2}}\sin\theta + F_S\frac{a^2\sqrt{1-e^2}}{a(1-e\cos E)}\right) \\
\frac{\mathrm{d}e}{\mathrm{d}t} &= \frac{h}{\mu}\sin\theta F_R + \frac{1}{\mu h}\left((h^2+\mu r)\cos\theta + \mu r\right)F_S \\
\frac{\mathrm{d}i}{\mathrm{d}t} &= \frac{r}{h}\cos(\omega+\theta)F_W \\
\frac{\mathrm{d}\Omega}{\mathrm{d}t} &= \frac{r}{h\sin i}\sin(\omega+\theta)F_W \\
\frac{\mathrm{d}\omega}{\mathrm{d}t} &= -\frac{1}{eh}\left(\frac{h^2}{\mu}\cos\theta F_R - (r+\frac{h^2}{\mu}\sin\theta F_S)\right) - \frac{r\sin\omega+\theta}{h\tan i}F_W \\
\frac{\mathrm{d}\theta}{\mathrm{d}t} &= \frac{h}{r^2} + \frac{1}{eh}\left(\frac{h^2}{\mu}\cos\theta F_R - (r+\frac{h^2}{\mu})\sin\theta F_S\right)
\end{aligned}
\tag{1.12}
$$

$$
\begin{aligned}
\frac{\mathrm{d}p}{\mathrm{d}t} &= \frac{2p}{w}\sqrt{\frac{p}{\mu}}F_R \\
\frac{\mathrm{d}f}{\mathrm{d}t} &= \sqrt{\frac{p}{\mu}}\left(F_R\sin L + [(w+1)\cos L + f]\frac{F_T}{w} - (h\sin L - k\cos L)\frac{gF_N}{w}\right) \\
\frac{\mathrm{d}g}{\mathrm{d}t} &= \sqrt{\frac{p}{\mu}}\left(-F_R\cos L + [(w+1)\sin L + g]\frac{F_T}{w} - (h\sin L - k\cos L)\frac{gF_N}{w}\right) \\
\frac{\mathrm{d}h}{\mathrm{d}t} &= \sqrt{\frac{p}{\mu}}\frac{s^2F_N}{2w}\sin L \\
\frac{\mathrm{d}k}{\mathrm{d}t} &= \sqrt{\frac{p}{\mu}}\frac{s^2F_N}{2w}\cos K \\
\frac{\mathrm{d}L}{\mathrm{d}t} &= \sqrt{\mu p}\left(\frac{w}{p}\right)^2 + \frac{1}{w}\sqrt{\frac{p}{\mu}}(h\sin L - k\cos L)F_N
\end{aligned}
\tag{1.13}
$$

Chapter 2

Dynamic Modelling

This section covers the kinetic modelling of a spacecraft in the vicinity of an asteroid. Throughout the mathematical description of the considered dynamics, design choices are motivated with regards their respective effects on simulation fidelity and computational complexity. The spacecraft's **rotational kinetics** can be modelled through the use of Newton's second law applied in the inertial frame (superscripted as "I") as $\frac{d}{dt}(\mathbf{I}^I\omega) = \mathbf{M}^I$. This is however not helpful as ω and I^I can change during the motion. Instead it is preferred to use Euler's equations describing the rotation of a rigid body, using a rotating reference frame attached to its principal axes of inertia:

$$\mathbf{I}\dot{\boldsymbol{\omega}} + \boldsymbol{\omega} \times (\mathbf{I}\boldsymbol{\omega}) = \mathbf{M}, \tag{2.1}$$

where, $\mathbf{I}$ = the inertia tensor,

$\dot{\omega}$ = the angular acceleration vector,

ω = the angular velocity vector,

$\mathbf{M}$ = the torque vector,

Expansion of Equation 2.1 in three-dimensional principle orthogonal coordinates gives

$$\begin{aligned} I_1\dot{\omega}_1 + (I_3 - I_2)\omega_2\omega_3 &= M_1, \\ I_2\dot{\omega}_2 + (I_1 - I_3)\omega_3\omega_1 &= M_2, \\ I_3\dot{\omega}_3 + (I_2 - I_1)\omega_1\omega_2 &= M_3. \end{aligned} \tag{2.2}$$

In physical reality, the instantaneous thrust control capabilities of a spacecraft are heavily dependent upon

Table 2.1: The effects of different accelerations on the final kinematic state of the NEAR Shoemaker spacecraft after being integrated with a fixed time-step (dt) of 100 s, of an interval of one orbital period with the initial Keplerian elements (a = 370 km) at an initial epoch at April 30, 2000 UTC (See **??**).

Case	$\lvert\mathbf{r}_e\rvert$ [m]	$\lvert\mathbf{v}_e\rvert$ [m/s]
Solar radiation pressure	1.512680e+04	4.319262e-02
Earth point mass	1.925349e-02	6.218576e-08
Moon point mass	2.371106e-04	7.674187e-10
Jupiter point mass	4.783348e-02	1.290854e-07
Mars point mass	2.175087e-04	6.178106e-10
Eros point mass	2.318650e+06	4.782929e-02

the current attitude of the spacecraft. This coupling is key in guidance strategies that ensure mission success in the short-term, such as docking in spacecraft rendezvous [**?**]. High model fidelity is always desirable, however the cost of modelling the rotational kinematics of a spacecraft is an approximate twofold expense in computational complexity. It is therefore common for the rotational kinematic modelling of a spacecraft to be assumed as decoupled from the translational kinematics for long-term horizon guidance and control strategies. Further motivation for the omission of the rotational kinematics is the *curse of dimensionality*, a term coined by Richard E. Bellman [**?**] [**?**]. This phenomena occurs in many domains and can be described as the effect of increased sparsity when increasing the dimensions of data, as less volume is filled by the data in the volume spanned by the increased dimensions. The spacecraft's **translational kinetics** can be effectively modelled using Newton's second law in the inertial frame as $\frac{d}{dt}(m\mathbf{v}^I) = \mathbf{F}^I$. There are a plethora of forces incident upon a spacecraft in interplanetary space, however a majority of their magnitudes are of such a low order that their effects can be considered negligible in most cases. This coupled with the fact that it is superfluous to model effects on the spacecraft's kinetics that are of magnitudes lower than than what is discernible with the navigation sensors. This extends to parameter estimation in that the magnitude of these effects would be negligible compared to measurement noise. Table 2.1 shows the effect of omitting specific acceleration models on the final state of an asteroid mission with the approximate parameters taken from the NEAR Shoemaker mission.

It is evident from Table 2.1 that the most influential effect on the kinetics of the spacecraft other than the trivial inclusion of the point-mass acceleration due to Eros within these mission parameters is the solar radiation pressure (SRP). It is therefore computationally beneficial, with minimal impact on the holistic result of the control and guidance, to exclude all sources of acceleration other than thrust, solar radiation pressure and the gravitational potential of the target asteroid.

As mentioned in subsection 1.1.5, the use of the RSW frame for thrust control provides significant insight into the effects incurred on the Keplerian elements of an orbit. In the same way that the effects of thrust in this frame provides meaningful insight to an astrodynamicist, it can be postulated that the learnability

may be improved for an arbitrary machine learning algorithm.

$$\begin{aligned}\ddot{\mathbf{r}} = \sum \mathbf{a}^I &= \mathbf{a}_g^I + \mathbf{a}_{SRP}^I + \mathbf{a}_T^I \\ &= \mathbf{R}^{I/B}\mathbf{a}_g^B + \mathbf{a}_{SRP}^I + \mathbf{R}^{I/RSW}\mathbf{a}_T^{RSW}\end{aligned} \tag{2.3}$$

where, $\mathbf{a}^I$ = an acceleration in the inertial frame (subsection 1.1.2),

$\mathbf{a}^B$ = an acceleration in the BCBF frame (subsection 1.1.4),

$\mathbf{a}^{RSW}$ = an acceleration in the RSW frame (subsection 1.1.5),

$\mathbf{R}^{Q/P}$ = rotation transformation from a frame P to Q,

$\mathbf{a}_g$ = the acceleration due to gravity of the asteroid,

$\mathbf{a}_{SRP}$ = the acceleration due to solar radiation pressure,

$\mathbf{a}_T$ = the acceleration due to thrust.

2.1. 1Solar Radiation Pressure

The simplest method of modelling the effect of solar radiation pressure without consideration for rotational kinetics can be done using a cannonball radiation model. This model assumes a constant radiation coefficient regardless of the orientation of the spacecraft with no torque effects. This behaviour is identical to that of an object that has spherically symmetric mass distribution, hence the term "cannonball". In inertial space $\{X_I\}$, this model is expressed as

$$\mathbf{a}_{SRP} = -\Xi P_\odot C_R \frac{A}{m}\frac{\mathbf{r}_\odot}{|\mathbf{r}_\odot|^3} AU^2 \tag{2.4}$$

where, Ξ = a 0 or 1 value, respectively the state of solar eclipse and incidence,

C_R = the coefficient of radiation pressure,

A = the reference area of solar incidence,

m = the instantaneous mass of the spacecraft,

$\mathbf{r}_\odot$ = the position vector of the Sun relative to the spacecraft,

AU = an astronomical unit (1.495978707×10^{11} m).

$P_\odot$ = the solar radiation pressure incident at 1 AU.

The state of whether to spacecraft is in solar eclipse or incidence can be determined through the combination of two conditions. An additional auxiliary vector is considered, the position of the Sun with

respect to the central body ($\mathbf{R}_\odot$). The first condition for eclipse is that the spacecraft orbital position around the central body ($\mathbf{r}_s$) has a component perpendicular to $\mathbf{R}_\odot$ (a) which exceeds the radius of the central body (R_e). This condition occurs when either the central body or spacecraft occults the other. A final check for which of these cases occurs is done by checking with the angle between $\mathbf{R}_\odot$ and $\mathbf{r}_s$ (Ψ) is acute or obtuse, that latter indicating that solar occultation is occuring for the spacecraft.

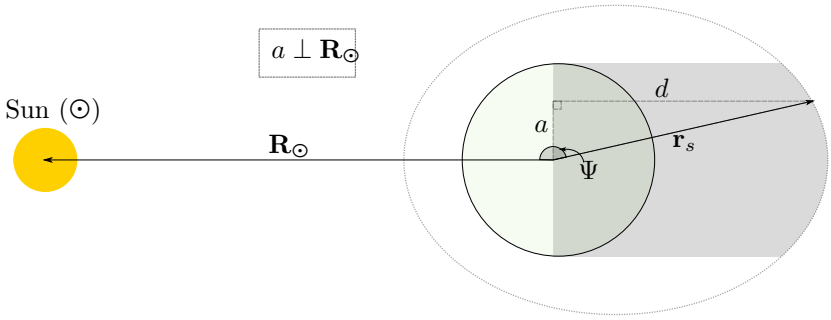

Figure 2.1: Illustration showing the geometry of a solar eclipse with respect to an orbiting spacecraft. The diagram is represented as a 2D cross-section parallel to the orbital plane.

The cosine of Ψ is determined and the sine of Ψ follows directly through trigonometric identities:

$$\cos\Psi = \frac{\mathbf{R}_\odot \cdot \mathbf{r}_s}{|\mathbf{R}_\odot||\mathbf{r}_s|}, \tag{2.5}$$

$$\sin\Psi = \sqrt{1-\cos^2\Psi}. \tag{2.6}$$

The combination of both conditions such that Ξ indicates the incidence of solar pressure on the spacecraft in logical operator notation is,

$$\Xi = \neg((\cos\Psi < 0) \wedge (r_s \sin\Psi < R_e)). \tag{2.7}$$

It should be noted that that is a simplification of reality, where in fact there are the regions of the umbra, penumbra and antumbra during eclipse, in decreasing order of solar incidence.

2.2. 1Thrust

The kinetics of the spacecraft are dependent on its instantaneous mass, seen in Newton's second law. The rate of change of mass of the spacecraft is given by the classical rocket equation

$$\dot{m} = -\frac{T}{I_{sp} \cdot g_0} \tag{2.8}$$

where, I_{sp} = the specific impulse of the propulsion system,

T = the net thrust supplied by the propulsion system,

g_0 = the standard gravity, which is nominally the gravity at Earth's surface.

The acceleration contribution due to thrust is then

$$\mathbf{a}_T = \frac{\mathbf{T}}{m}. \tag{2.9}$$

2.3. 1Gravitational Potential

The acceleration due the gravitational potential of a body in inertial space $\{X^I\}$ is expressed as,

$$\begin{gathered} \mathbf{a}_g^I = \mathbf{R}^{I/B} \nabla_{\mathbf{r}} U(\mathbf{r}^B) \\ \text{replacing Equation 1.3: } \mathbf{a}_g^I = \mathbf{R}_z(W)\mathbf{R}_x(\pi/2 - \delta_0)\mathbf{R}_z(\pi/2 - \alpha_0)\nabla_{\mathbf{r}} U(\mathbf{r}^B) \end{gathered} \tag{2.10}$$

where, $\nabla_{\mathbf{r}} U(\mathbf{r})$ = the vector differential of the gravitational potential field,

W = the ephemeris position of the prime meridian (Equation 1.2),

α_0, δ_0 = ICRF equatorial coordinates (right ascension & declination) at epoch J2000.0.

The transformation from body-fixed coordinates into the inertial frame is emphasised in Equation 2.10 to make clear the temporal coupling of a potential field in inertial space. For a spherically symmetric potential, such as the point mass approximation, only the relative position to the body in inertial space is needed. This coupling plays a part in defining the equator of date and the ephemeris position of the prime meridian, which together define the body-fixed coordinate system of the considered body. When the evolution of the rotation axis is ignored, this coupling results in five base characteristic parameters of the gravitational potential field in inertial space when processing Earth-based observations: W_0, $\dot{W}$, α_0, δ_0 and $\mathbf{r}^{I/B}$. For the remainder of this section on gravitational potential, the body-fixed coordinate $\mathbf{r}^B$ will be referred to as $\mathbf{r}$ for simplicity. As noted by by Montenbruck Gill [?], the gravitational potential may be generalised to an arbitrary mass distribution through the summation of all contributions of individual mass elements, with $dm = \rho(\mathbf{r}')d^3\mathbf{r}'$,

$$U(\mathbf{r}) = G \int_V frac\rho(\mathbf{r}')|\mathbf{r} - \mathbf{r}'|\, d^3\mathbf{r}' \tag{2.11}$$

where, G = the universal gravitational constant $(6.6695 \times 10^{11}[\mathrm{m}^3 \cdot \mathrm{kg}^{-1} \cdot \mathrm{s}^{-2}])$

$\mathbf{r}$ = position at which potential is calculated,

$\mathbf{r}'$ = position of point inside the body mass,

$\rho(\mathbf{r}')$ = density at given point inside the body mass.

The acceleration contribution due to gravity is related to gravitational potential through $\mathbf{a}_g = \nabla_{\mathbf{r}} U$.

A. 1Point mass

The lowest fidelity gravitational potential model that can be used in estimation is a point-mass approximation to gravitational potential,

$$U(r) = \frac{GM}{r} \tag{2.12}$$

where, M = mass of the primary body generating the potential field.

This model has the main advantage that it is decoupled from the body-fixed coordinate system, reducing the number of estimated parameters required for a first order approximation of the mass of a the considered body. The acceleration contribution due to gravity is then,

$$\boldsymbol{a}_g = \begin{bmatrix} a_{g_x} \\ a_{g_y} \\ a_{g_z} \end{bmatrix} = \nabla_{\mathbf{r}} U = \begin{bmatrix} \frac{\partial U}{\partial x} \\ \frac{\partial U}{\partial y} \\ \frac{\partial U}{\partial z} \end{bmatrix} = \begin{bmatrix} -\frac{GM}{{r_x}^2} \\ -\frac{GM}{{r_y}^2} \\ -\frac{GM}{{r_z}^2} \end{bmatrix} \tag{2.13}$$

B. 1Tri-axial ellipsoid: elliptical integrals

An alternative lower fidelity model of a body is the use of a tri-axial ellipsoid of homogenous mass distribution. This approach assumes the small body's density (ρ) as uniform, which allows the gravitational parameter (μ) of the body to be expressed as,

$$\mu = GM = G\rho\frac{4}{3}\pi abc. \tag{2.14}$$

This model is illustrated in Figure 2.2 with $I_x < I_y < I_z$. This model corresponds to the convention of body-fixed frames which have their Z-axis aligned with the rotational axis of the body, however due to

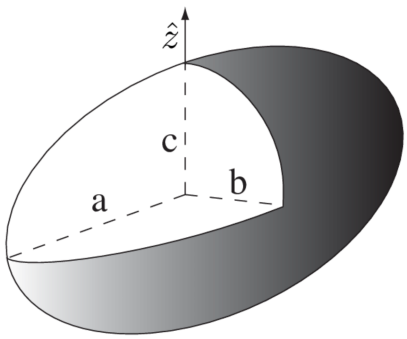

Figure 2.2: Tri-axial ellipsoid model of homogeneous mass distribution ρ, with $I_x < I_y < I_z$, respectively with axes a, b, and c.

precession and nutation, the true Z-axis of date representing the current rotation axis will differ from the geometrical $\hat{Z}$-axis of the tri-axial ellipsoid. The period of precession and nutation for short time scales however can be omitted and for studies which does not involve long term analysis of the subsequent effects, $Z \approx \hat{Z}$. There is a closely related model which is the next step taken by astrodynamacists after a point mass approximation in missions design, which is the use of an oblate spheroid. This is often used to account for the mass concentration at the equator of Earth. This model is obtained from the homogeneous tri-axial ellipsoid by simply setting $b = a$. The gravitational potential, U, using this model with elliptical integrals, of a body in its body-fixed reference frame $\{X^B\}$ is

$$U(\mathbf{r}) = \frac{3}{4}\mu \int_{\kappa_0}^{\infty} \left(1 - \frac{{r_x}^2}{a^2+\kappa} - \frac{{r_y}^2}{b^2+\kappa} - \frac{{r_z}^2}{c^2+\kappa}\right) \cdot \frac{d\kappa}{\sqrt{((a^2+\kappa)(b^2+\kappa)(c^2+\kappa))}} \tag{2.15}$$

where, κ = parameter of the pencil for a confocal ellipse

κ_0 = largest root of the confocal ellipsoid

a, b, c = length of ellipsoid axes, respectively in the x, y and z directions of the body-fixed frame $\{X^B\}$.

$$C(\kappa) = \frac{{r_x}^2}{a^2+\kappa} + \frac{{r_y}^2}{b^2+\kappa} + \frac{{r_z}^2}{c^2+\kappa} - 1. \tag{2.16}$$

The expressions above are attributed to [**?**], a detailed derivation is given by Mac Millan [**?**], Danby [**?**] and Moulton [**?**]. The integrals seen in Equation 2.15 are elliptic integrals. By use of Legendre's canonical elliptic integrals of first kind F and second kind E, it is possible to find an expression for U and it's derivatives. Alternatively, as demonstrated by Willis et al. [**?**], a more modern approach using Carlson

elliptic integrals. After introducing $\kappa' = \kappa - \kappa_0$ in **??**, the gravitational potential becomes,

$$\begin{aligned} U(\mathbf{r}) = & \frac{3}{2}\mu R_F(a^2+\kappa_0, b^2+\kappa_0, c^2+\kappa_0) \\ & - \frac{1}{2}\mu {r_x}^2 R_D(b^2+\kappa_0, c^2+\kappa_0, a^2+\kappa_0) \\ & - \frac{1}{2}\mu {r_y}^2 R_D(a^2+\kappa_0, c^2+\kappa_0, b^2+\kappa_0) \\ & - \frac{1}{2}\mu {r_z}^2 R_D(a^2+\kappa_0, b^2+\kappa_0, c^2+\kappa_0), \end{aligned} \tag{2.17}$$

where $R_F(x,y,z)$ and $R_D(x,y,z)$ are two of the Carlson symmetric forms, and their incomplete elliptic integrals are

$$R_F(x,y,z) = \frac{1}{2}\int_0^\infty \frac{dt}{\sqrt{(t+x)(t+y)(t+z)}}, \tag{2.18}$$

$$R_D(x,y,z) = \frac{3}{2}\int_0^\infty \frac{dt}{(t+x)\sqrt{(t+x)(t+y)(t+z)}}. \tag{2.19}$$

The numerical evaluation of the above expressions (Equation 2.18 and Equation 2.19) are detailed by Johansson [**?**]. The acceleration due to the gravitational potential then becomes:

$$\boldsymbol{a}_g = \begin{bmatrix} a_{g_x} \\ a_{g_y} \\ a_{g_z} \end{bmatrix} = \nabla_{\mathbf{r}} U = \begin{bmatrix} \frac{\partial U}{\partial x} \\ \frac{\partial U}{\partial y} \\ \frac{\partial U}{\partial z} \end{bmatrix} = \begin{bmatrix} \mu r_x R_D(b^2+\kappa_0, c^2+\kappa_0, a^2+\kappa_0) \\ \mu r_y R_D(a^2+\kappa_0, c^2+\kappa_0, b^2+\kappa_0) \\ \mu r_z R_D(a^2+\kappa_0, b^2+\kappa_0, c^2+\kappa_0) \end{bmatrix} \tag{2.20}$$

C. 1Expansion in spherical harmonics

The general approach for high fidelity gravitational potential modelling is the use of spherical harmonic expansion. The gravitational potential, U, of a body, in its body-fixed reference frame $\{X^B\}$ is described by the infinite series

$$U(r,\phi,\lambda) = \frac{GM}{r}\sum_{n=0}^{\infty}\sum_{m=0}^{n}\left[\left(\frac{R}{r}\right)^l \times \overline{P}_{nm}(\sin\phi)(\overline{C}_{nm}\cos m\lambda + \overline{S}_{nm}\sin m\lambda)\right], \tag{2.21}$$

where, r, ϕ, λ = spherical coordinates in $\{X^B\}$, respectively the radius coordinate, latitude and longitude,

G = universal gravitational constant,

M = mass of body,

n, m = respectively the degree and order of a particular spherical harmonic,

R = reference radius,

$\overline{P}_{nm}$ = the normalized associated Legendre polynomials,

$\overline{C}_{nm}, \overline{S}_{nm}$ = the normalized spherical harmonic coefficients,

This expansion is infinite in priciple and may be truncated in practice depending on the degree of knowledge of the body surface or gravitational potential field. The degree and order to which the spherical harmonics are expanded are determined by the quantity and quality of empirical observations. These observations constrain the the certainty associated to the harmonic coefficients in the expansion. The general approach is to fit higher fidelity expansions, until the residual error between observation and model converge towards a random normal distribution. This convergence suggests that only stochastic error sources remain, which cannot be modelled deterministically. These error sources are usually due to the limitation of the hardware employed in the collection of measurements.

D. 1Tri-axial ellipsoid: expansion in spherical harmonics

The expansion in spherical harmonics may be easily expanded to represent a homogeneous distribution of mass as a tri-axial ellipsoid, providing a bridge to the elliptic integral representation presented previously. This expansion is demonstrated by Balmino [**?**]. After introducing the mass $M = \frac{4}{3}\pi abc\rho$, it is demonstrated that,

$$\begin{aligned} C_{2l,2m} = & \frac{3}{R^{2l}} \frac{l!(2m)!}{2^{2l}(2l+3)(2l+1)!}(2-\delta_{0m})\frac{(2l-2m)!}{(2l+2m)!} \\ & \times \sum_{k=0}^{l-m} \frac{(-1)^k(4l-2k)!}{(2l-k)!(2l-2m-2k)!} \\ & \times \sum_{s=0}^{m} \frac{(-1)^s}{(2s)!(2m-2s)!} \sum_{p=0}^{k} \frac{(2l-2m-2p)!}{(l-m-p)!(k-p)!} \\ & \times \sum_{q=0}^{p} \frac{(2s+2p-2q)!(2m-2s+2q)!}{q!(p-1)!(s+p-q)!(m-s+q)!} \\ & \times a^{2(m-s+q)} b^{2(s+p-q)} c^{2(l-m-p)}, \end{aligned} \tag{2.22}$$

where, for example, it is found that,

$$\begin{aligned} C_{20} &= \frac{1}{5R^2}\left(c^2 - \frac{a^2+b^2}{2}\right), \\ C_{22} &= \frac{1}{20R^2}(a^2-b^2), \\ C_{40} &= \frac{15}{7}(C_{20}^2 + 2C_{22}^2), \\ C_{42} &= \frac{5}{7}C_{20}C_{22}, \\ C_{44} &= \frac{5}{28}C_{22}^2. \end{aligned} \tag{2.23}$$

It is further noted by Balmino [**?**] that there is a uniform convergence condition for Equation 2.21 in the case of the homogenous tri-axial ellipsoid equivalent expansion, which is $a < c\sqrt{2}$.

2.4. 1Numerical Analysis

A. 1Initial value problems

B. 1Integration methods

C. 1Mesh refinement

1Reducing element size: h-method

1Increasing element order: p-method

1Optimising element location: r-method

D. 1Interpolation methods

Chapter 3

Trajectory Optimization

Trajectory optimisation is the process of designing a series of states across a temporal dimension that maximizes (or minimizes) a measure of performance. This technique is generally used to obtain the open-loop solution of an optimal control problem within a finite horizon. Due to the common presence of nonlinearities in the constraint and/or performance functions, trajectory optimisation problems often employ the use of *nonlinear programming*.

Mathematicaly the problem can be described by N phases, with the independent variable t, where phase k lies within the region $t_0^{(k)} \leqslant t \leqslant t_f^{(k)}$. The independent variable t very often describes time within mosr practical applications, where the phases are sequential, that is $t_0^{(k+1)} = t_f^{(k)}$, however as stated by *Betts*, and demononstrated well by section 3.2, neither of these assumptions are required. In phase k, the dynamic variables are described as,

$$\mathbf{z} = \begin{bmatrix} \mathbf{x}^{(k)}(t) \\ \mathbf{u}^{(k)}(t) \end{bmatrix}, \tag{3.1}$$

where $\mathbf{x}_k$ and $\mathbf{u}_k$ describe the *state variables* and *control variables* respectively at the n knot points. bash -ic -file-line-error -interaction=nonstopmode -synctex=1 -output-format=pdf "-output-directory=/mnt/c/Users/ggarr/Onel Study/out"/mnt/c/Users/ggarr/OneDrive/Documents/Literature Study/main.tex

3.1. 1Sims-Flanagan Method

A common method for low-thrust trajectory optimisation in numerical astrodynamics, the Sims-Flanagan method [**?**], is the optimisation of a low-thrust trajectory following transcription into a series of conic arcs connected by ΔV impulses, as seen in Figure Figure **??**.

This method is fast and robust, however due to its discretization of a continuous low-thrust problem, it can fail to be a faithful representation of reality. Yam et al. improve upon this method in two ways: 1) the

ΔV impulses are replaced with continuous thrust where the low-thrust arcs are numerically propagated; and 2) the time mesh, or series of knot points, are optimised together with the trajectory.

3.2. 1Sundmann Transform

Karl Sundman introduced a simple transformation for the time variable, to regularize the otherwise singular three body problem. A new variable s is introduced through the relation $ds = dt/r$ which *guarantees an asymptotically slower flow* near the singularities [?].

$$
\begin{aligned}
r &= \sqrt{x_1^2 + x_2^2 + x_3^2} \\
\dot{x}_1 &= x_4 r \\
\dot{x}_2 &= x_5 r \\
\dot{x}_3 &= x_6 r \\
\dot{x}_4 &= -x_1/r^2 + u_1 r \\
\dot{x}_5 &= -x_2/r^2 + u_2 r \\
\dot{x}_6 &= -x_3/r^2 + u_3 r \\
\dot{t} &= r
\end{aligned}
\tag{3.2}
$$

Yam et al. demonstrates quite effectively that sampling in the s domain is useful for trajectory optimization. [?] The difference between equal sampling in the s domain compared to that of time, is seen in Figure **??**.

It is evident from Figure **??** that sampling the s domain is superior in generating a smooth trajectory, in the context of orbital trajectory discretization. This presents an interesting aspect when one considers replacing the temporal variable of time with the s-domain in the context of an infinite-horizon reinforcement learning problem.

3.3. 1Optimal Control

A. 1Potryagins maximum principal

B. 1Model predictive control (MPC)

C. 1Recent Research

1Autoencoder of coordinates

`https://www.youtube.com/watch?v=KmQkDgu-Qp0`

3.4. 1Linearization

Given the complexity of the models which depend on a variety of parameters which are used in the description of the dynamic motion or measurement process, it is customary to linearize the relations between observables and the independent parameters in order to obtain expressions which are more easily handled.

A. 1Taxonomy of Partials

1The State Transition Matrix

Let the state vector $\mathbf{y}(\mathbf{t})$ of the dynamic system at an arbitrary epoch t be the concatenation of the position $\mathbf{r}(t)$ and velocity vector $\mathbf{v}(t)$. A state vector at a specified epoch is given by $\mathbf{y}(t_0)$. The state transition matrix $\mathbf{\Phi}(t, t_0)$ describes the change of the state vector at a time t due to a change in the initial state vector at time t_0

$$\left(\frac{\partial \mathbf{y}(t)}{\partial \mathbf{y}(t_0)}\right)_{6\times 6} = \mathbf{\Phi}(t, t_0). \tag{3.3}$$

1The Sensitivity Matrix

For a given set of n_p parameters which are dependent variables in the calculation of acceleration acting on on the system of bodies $\mathbf{p}$, their dependence is described by the sensitivity matrix, i.e. the partial derivatives

$$\left(\frac{\partial \mathbf{y}(t)}{\partial \mathbf{p}}\right)_{6\times n_p} = \boldsymbol{S}(t) \tag{3.4}$$

with respect to the force model parameters. The parameters p often include coefficients which are empirical in nature, these include but are not limited to the coefficients of lift, drag, and radiation pressure.

1Partials of measurements with respect to the state vector

The linearized dependence of

B. 1Solar Radiation Pressure

1Partial derivative with respect to state

$$\frac{\partial \boldsymbol{a}_s}{\partial \mathbf{r}} = -P_{\odot}\frac{A}{m}\frac{AU^2}{r^5}\begin{bmatrix} 3r_x^2 - r^2 & 3r_x r_y & 3r_x r_z \\ 3r_y r_x & 3r_y^2 - r^2 & 3r_y r_z \\ 3r_z r_x & 3r_z r_y & 3r_z^2 - r^2 \end{bmatrix} \tag{3.5}$$

1Partial derivative with respect to coefficient of radiation pressure

$$\frac{\partial \boldsymbol{a}_s}{\partial C_r} = \frac{1}{C_R}\boldsymbol{a}_s = -P_{\odot}\frac{A}{m}\frac{\mathbf{r}}{r^3}AU^2 \tag{3.6}$$

C. 1Thrust

$$\frac{\boldsymbol{a}_T}{\partial} \tag{3.7}$$

D. 1Gravitational Potential: Point Mass

1Partial derivative with respect to state

$$\frac{\partial \boldsymbol{a}_g}{\partial \mathbf{r}} = \frac{\mu}{r^5}\begin{bmatrix} 3r_x^2 - r^2 & 3r_x r_y & 3r_x r_z \\ 3r_y r_x & 3r_y^2 - r^2 & 3r_y r_z \\ 3r_z r_x & 3r_z r_y & 3r_z^2 - r^2 \end{bmatrix} \tag{3.8}$$

1Partial derivative with respect to gravitational parameter

$$\frac{\partial \boldsymbol{a}_g}{\partial \mu} = \frac{1}{\mu}\boldsymbol{a}_g = -\frac{\mathbf{r}}{r^3} \tag{3.9}$$

E. 1Gravitational Potential: Tri-axial ellipsoid

1Partial derivative with respect to state

$$\frac{\partial \boldsymbol{a}_g}{\partial \mathbf{r}} = \not{\mu}\left[\tag{3.10}$$

1Partial derivative with respect to characteristic parameters

$$\mathbf{p}_g = \begin{bmatrix} \rho & a & b & c \end{bmatrix}^T \tag{3.11}$$

$$j_1 = \tag{3.12}$$

$$\frac{\partial \boldsymbol{a}_g}{\partial \rho} = G\frac{4}{3}\pi \begin{bmatrix} abcr_x R_D(b^2+\kappa_0, c^2+\kappa_0, a^2+\kappa_0) \\ abcr_y R_D(a^2+\kappa_0, c^2+\kappa_0, b^2+\kappa_0) \\ abcr_z R_D(a^2+\kappa_0, b^2+\kappa_0, c^2+\kappa_0) \end{bmatrix} \tag{3.13}$$

$$\frac{\partial \boldsymbol{a}_g}{\partial \mathbf{p}_g} = G\frac{4}{3}\pi \begin{bmatrix} abcr_x R_{D_x} & \rho bc(r_x R_{D_x} + a\frac{\partial R_{D_x}}{\partial a}) & \rho ac(r_x R_{D_x} + b\frac{\partial R_{D_x}}{\partial b}) & \rho ab(r_x R_{D_x} + c\frac{\partial R_{D_x}}{\partial c}) \\ abcr_y R_{D_y} & \rho bc(r_y R_{D_y} + a\frac{\partial R_{D_y}}{\partial a}) & \rho ac(r_y R_{D_y} + b\frac{\partial R_{D_y}}{\partial b}) & \rho ab(r_y R_{D_y} + c\frac{\partial R_{D_y}}{\partial c}) \\ abcr_z R_{D_z} & \rho bc(r_z R_{D_z} + a\frac{\partial R_{D_z}}{\partial a}) & \rho ac(r_z R_{D_z} + b\frac{\partial R_{D_z}}{\partial b}) & \rho ab(r_z R_{D_z} + c\frac{\partial R_{D_z}}{\partial c}) \end{bmatrix} \tag{3.14}$$

F. 1Gravitational Potential: Expansion in spherical harmonics

3.5. 1Observation Models

A. 1Landmark Tracking

Marie's Thesis + Michael. Model is similar to VLBI model.

2.1.1 In D.Dirkx for better notation.

Moyer, formulation for observed and computed quantities in DSN types.

B. 1Range Measurements/ Pseudorange

C. 1Doppler Measurements

1Two-way Range Rate

$$\bar{\dot{\rho}}(t) = \frac{c}{2}\frac{(\tau_{2u} + \tau_{2d}) - (\tau_{1u} + \tau_{2d})}{t_c} = \frac{1}{2}\frac{(\rho_{2u} + \rho_{2d}) - (\rho_{1u} + \rho_{1d})}{t_c}, \tag{3.15}$$

1Range

1One-Way Range Rate

$$\bar{\dot{\rho}} = c\frac{(\tau_2 - \tau_1)}{t_c} = \frac{(\rho_2 - \rho_1)}{t_c} \tag{3.16}$$

1Rational Doppler Bias

No real need to discuss, cut out in post processing.

$$\delta\bar{\dot{\rho}} = \frac{1}{t_c}\int_{t-t_c}^{t} d \cdot \omega \sin\alpha \sin\omega t \; dt \tag{3.17}$$

$$\Delta\bar{\dot{\rho}} = \frac{\lambda\omega}{2\pi}\frac{s_R + s_T/T_{1,2}}{2} \tag{3.18}$$

3.6. 1Parameter Estimation

- Orbit of asteroid
- Orbit of spacecraft
- Rotation of asteroid (rate + principle axes)
- Gravitational potential of asteroid

A. 1Orbit Determination

1Weighted Least-Squares Estimation

$$H = \frac{\partial \mathbf{h}}{\partial \mathbf{q}} \tag{3.19}$$

$$\Delta \mathbf{q} = K(H^T W \Delta \mathbf{h}) \tag{3.20}$$

$$K = (H^T W H)^{-1} \tag{3.21}$$

1Linearization & Normal Equations

1Filtering

A CEKF consists of 3 main steps, namely: *Initialisation (0)*, *Prediction (1)* and *Correction (2)*, where steps 1 & 2 are iterated through $K-1$ times, where K ($K \in \mathbb{Z}^+$) quantifies the number of Epochs.

- **Step (0) Initialisation**: The *a posteriori* estimate of the initial state ($\hat{x}_0^+$) is determined according to the expectation of the true value x_0. The initial state error co-variance matrix is calculated according to the expectation of the co-variance between $\hat{x}_0^+$ and x_0. Within the context of satellite tracking, a predefined $\hat{x}_0^+$ will be used throughout the CEKF analysis to analyse the performance as a result of the selection of hyper-parameters: $\boldsymbol{Q}_{k-1}$ and $\boldsymbol{R}_k$.
- **Step (1) Prediction**: Project the state and its co-variance matrix at $k-1$ one step forward in order to obtain the *a priori* estimates at k according to the system dynamics. $\boldsymbol{Q}_{k-1}$ is implemented, then this contributes to the *a priori* estimate of P_k.
- **Step (2) Correction**: The measurements at k are then compared with the predicted state according to system dynamics (*a priori* estimate) providing the *measurement innovation* ($\Delta\rho_k$). *innovation co-variance* (S_k) and H_k are then calculated and used to obtain the *Kalman gain* ($\overline{K}_k$). Finally

the *a posteriori* estimate of the state ($\hat{x}_k^+$) and co-variance (P_k^+) are determined. k is incremented by a step forward and the process from step 1 is repeated for all Epochs.

$$\rho = ||\mathbf{r}_\odot - \mathbf{R}_\oplus|| \tag{3.22}$$

$$\rho = ||\mathbf{r}_\odot - \mathbf{R}_\oplus|| \tag{3.23}$$

- **Orbit Determination**
-

B. 1Rotational State

C. 1Gravitational Potential

D. 1Shape

- **Rotation Model**:

Figure 3.1: Impulsive ΔV transcription of a low-thrust trajectory, after Sims and Flanagan [?].

Figure 3.2: A trajectory sampled with the same number of a) time spaced segments b) s-spaced segments [?].

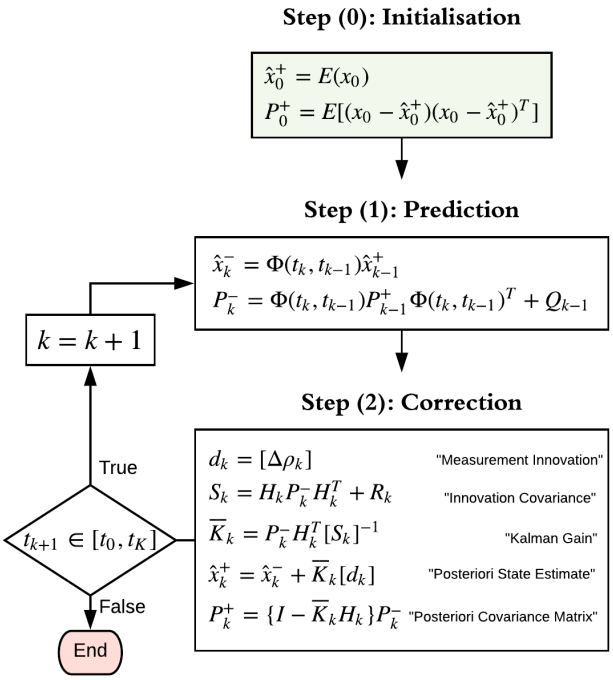

Figure 3.3: CEKF flow diagram for process of tracking and data prediction including all equations [?].

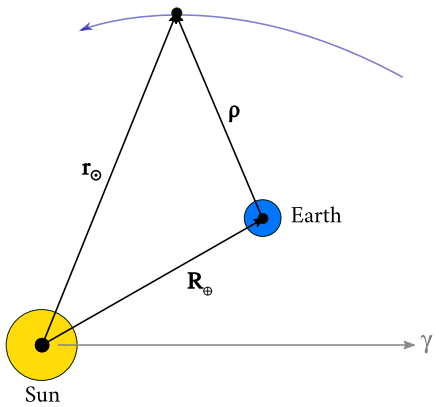

Figure 3.4: Orbit determination of asteroid using range observations from Earth (ρ).

Chapter 4

Machine Learning

Machine learning, often described as a proper subset of artificial intelligence [**?**], and is the field in computer science which deals with the improvement of algorithms through experience and the use of data [**?**]. Our daily lives exhibit wide applications of intelligent software to automate routine labour, understand speech or images, assist in diagnoses in medicine and support basic scientific research. This field as a whole is relatively young, having been coined in 1959 by Arthur Samuel [**?**], however little progress in reaching human-comparable learning was achieved until the advent of deep learning, termed by Rina Dechter in 1986 [**?**]. Even then, human-like recognition of real-world images was not achieved until ImageNet was created in 2009 [**?**], which is often considered as the catalyst for the AI boom of the 21st century [**?**].

This section reviews the current ongoing research in the field of machine learning as a whole. First the main categories: *Supervised learning*, *Unsupervised learning*, *Semi-supervised learning*, and *Reinforcement learning* are distinguished with examples in section 4.1. The biggest contributing technique to the field as a whole: deep learning, predominantly part of supervised learning, is reviewed in section 4.2. Finally, the category of reinforcement learning is reviewed in section 4.3.

4.1. 1Categories of Machine Learning

Tasks provided to machine learning algorithms have different formulations based on the problem being addressed. These categories of tasks are most distinct by the method by which the algorithm is provided further experience, or data, from which it is expected to learn some pattern. These are defined by the following main categories:

- **Supervised learning** is the machine learning task of learning a mapping between an input **x** to an output **y** based on example input-output pairs, otherwise referred to as the labelled training

data consisting of a set of training examples. The trained *model* is then provided an unseen x for which it must estimate y based on its experience. Supervised models are further grouped into two subcategories, classification and regression. **Classification** is the task of mapping x to a discrete output variable y which determines the predicted class based on the x. A simple example of this would be a y in $\mathbb{R}^2$ which determines whether the input image was a *cat* or a *dog*. **Regression** is task of mapping x onto a continuous output variable y which determines the value of some variable of interest. An example of this would be the task of learning an approximator to the function: $f(x) = x^2$.

- **Unsupervised learning** involves the task of learning relations between input data, x with no labels, y provided. This form of learning often deal with pattern recognition problems in *association* & *clustering* [**?**].

- **Semi-supervised** is a middle ground between supervised learning (in which all training data is labelled) and unsupervised learning (in which no label data is provided) [**?**]. Some example applications of this paradigm are dimensionality reduction [**?**], clustering [**?**], and anomaly detection [**?**].

- **Reinforcement learning** is a learning task which relies exclusively on a series of reinforcements. These reinforcements can be positive (rewards) or negative (punishments). This category is discussed further in section 4.3.

4.2. 1Deep Learning

A. 1The fundamental component: Perceptrons

Proposed by Rosenblatt [**?**] in his technical report funded by the United States Office of Naval Research [**?**] in 1957, the *perceptron* is a fundamental component of deep learning, describing a mathematical model of a biological neuron. There are two different sets of notation which exist when dealing with the bias of a perceptron. One involves the inclusion of a unit constant in the input vector $\mathbf{x}$, with the bias being specified by the value of the first weight w_0. An alternative notation exists which treats the bias as a standalone value b. The latter notation will be used, as it is the preferred notation in contemporary deep learning papers. The notation defining the mapping of a perceptron is then: $f(\mathbf{x}; \mathbf{w}, b) = \mathbf{x}^T\mathbf{w} + b$; $x \in \mathbb{R}^{d_{in}}$, $\mathbf{w} \in \mathbb{R}^{d_{in}}$, $b \in \mathbb{R}$.

This mathematical mimicry of a biological neuron was first used used proposed by Rosenblatt where a set of inputs $\mathbf{x}$ weighted using $\mathbf{w}$ before being summed. If this sum surpassed a threshold, then a binary output of 1 was returned. Figure 4.1 shows a more general formulation which applies to the resulting field of deep learning, with any activation function ϕ analogous for the level of excitation of a biological

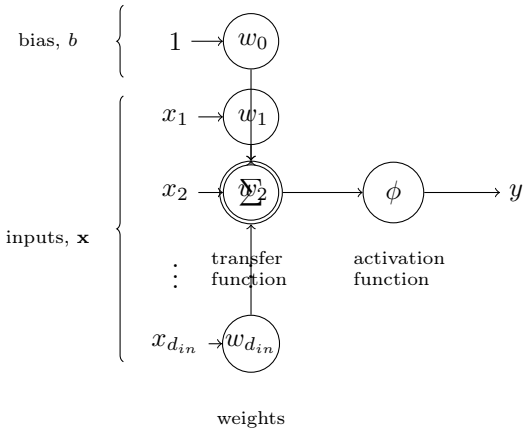

Figure 4.1: Perceptron

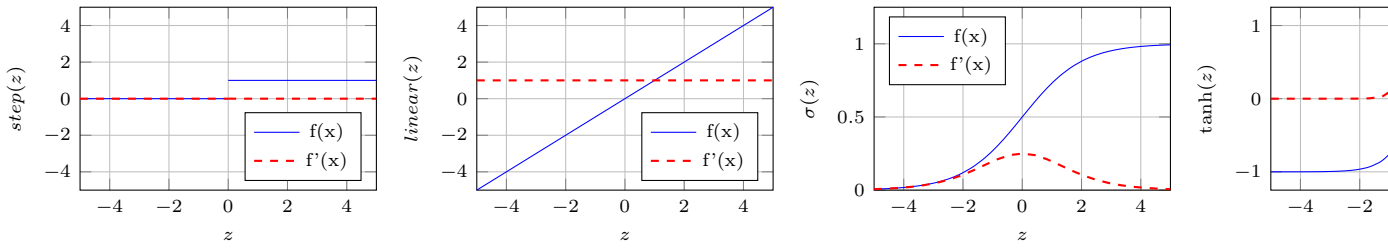

(a) Threshold Step (b) Linear (c) Sigmoid (d) Hyperbo

Figure 4.2: Commonly used activation functions in MLPs.

neuron in response to its stimulus **x**.

The primary criticism of the perceptron came in 1969 from Minsky and Papert [**?**], where it was shown that the perceptron could only solve *linearly separable* functions, and failed to solve the XOR and NXOR functions. They went on to claim that the research being done was doomed to failure due to these limitations, resulting in little research in the area being done until about the 1980's.

B. 1Activation function

Since the early days of the perceptron, a wide variety of activation functions ϕ have been used and improve upon the threshold step function.

C. 1Multilayer perceptrons, a.k.a feed forward networks

$f(\mathbf{x}; \mathbf{w}, b) = \mathbf{x}^T\mathbf{w} + b$; $x \in \mathbb{R}^{d_{in}}$, $\mathbf{w} \in \mathbb{R}^{d_{in}\times}$, $b \in \mathbb{R}^1$.

$$\mathbf{h}^{(1)} = g^{(1)}\left(\mathbf{W}^{(1)T}\mathbf{x} + \mathbf{b}^{(1)}\right); \tag{4.1}$$

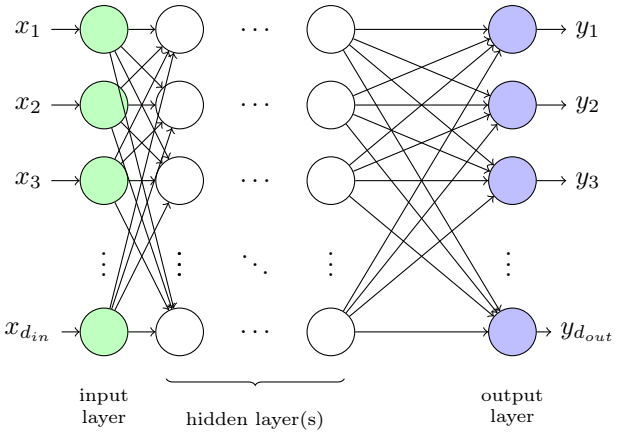

Figure 4.3: Multilayer perceptron

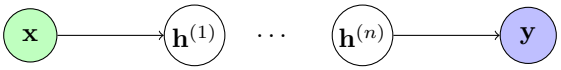

Figure 4.4: Multilayer perceptron

$$\mathbf{h}^{(2)} = g^{(2)}\left(\mathbf{W}^{(2)T}\mathbf{h}^{(1)} + \mathbf{b}^{(2)}\right); \tag{4.2}$$

D. 1Gradient based learning

E. 1Universal Approximation Properties and Depth

A linear model by definition, may only optimised to represent linear functions. It has advantages in its simplicity to optimise however we often require our estimator models to learn nonlinear functions.

F. 1Backpropagation

Backpropagation, short for "backward propagation of errors," is a *supervised learning* algorithm for artificial neural networks using *gradient descent*.

4.3. 1Reinforcement Learning

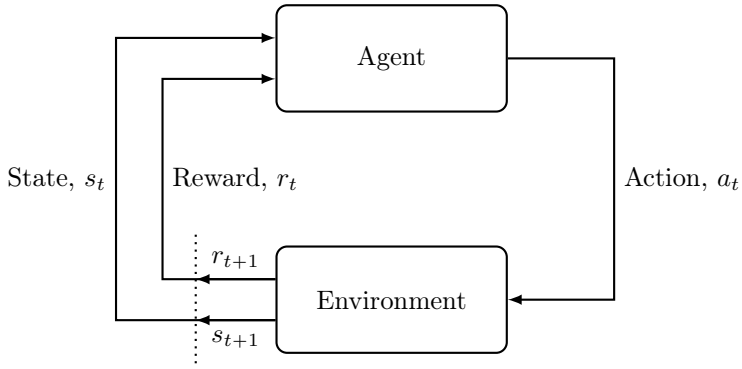

Figure 4.5: Agent-environment interaction interface.

- states and observations,
- action spaces,
- policies,
- trajectories,
- different formulations of return,
- the RL optimization problem,
- and value functions.

A. 1Taxonomy of Reinforcement Learning

B. 1Value-based methods

C. 1Policy-based methods

D. 1Policy gradient

E. 1Deep deterministic policy gradient (DDPG)

1Appendix A: Mathematical Expressions

1Rotation transformations

$$\mathbb{T}_x(\phi_x) = \begin{bmatrix} 1 & 0 & 0 \\ 0 & \cos\phi_x & \sin\phi_x \\ 0 & -\sin\phi_x & \cos\phi_x \end{bmatrix} \tag{3}$$

$$\mathbb{T}_y(\phi_y) = \begin{bmatrix} \cos\phi_y & 0 & -\sin\phi_y \\ 0 & 1 & 0 \\ -\sin\phi_y & 0 & \cos\phi_y \end{bmatrix} \tag{4}$$

$$\mathbb{T}_z(\phi_z) = \begin{bmatrix} \cos\phi_z & \sin\phi_z & 0 \\ -\sin\phi_z & \cos\phi_z & 0 \\ 0 & 0 & 1 \end{bmatrix} \tag{5}$$

1Incomplete integrals

$$U(r_x, r_y, r_z) = G\int_V \frac{\rho(s_x, s_y, s_z)}{\sqrt{(r_x - s_x)^2 + (r_y - s_y)^2 + (r_z - s_z)^2}}\, dx\, dy\, dz \tag{6}$$

$$R_F(x, y, z) = \frac{1}{2}\int_0^\infty \frac{1}{\sqrt{t + x}\sqrt{t + y}\sqrt{t + z}}\, dt \tag{7}$$

$$R_D(x, y, z) = \frac{3}{2}\int_0^\infty \frac{1}{(t + x)\,(t + y)\,(t + z)^{3/2}}\, dt \tag{8}$$

1Appendix B

1Conversions of Orbital Elements

1Modified Equinoctial to Keplerian

$$a = \frac{p}{1 - f^2 - g^2} \tag{9}$$

$$e = \sqrt{f^2 + g^2} \tag{10}$$

$$i = 2\tan^{-1}\sqrt{h^2 + k^2} = \text{atan2}(2\sqrt{h^2 + k^2}, 1 - h^2 - k^2) \tag{11}$$

$$i = 2\tan^{-1}\sqrt{h^2 + k^2} = \text{atan2}(2\sqrt{h^2 + k^2}, 1 - h^2 - k^2) \tag{12}$$

$$\omega = \tan^{-1}(g/f) - \tan^{-1}(k/h) = \text{atan2}(gh - fk, fh + gk) \tag{13}$$

$$\Omega = \text{atan2}(k, h) \tag{14}$$

$$\theta = L - (\Omega + \omega) = L - \tan^{-1}(g/f) \tag{15}$$

$$u = \omega + \theta = \text{atan2}(h\sin L - k\cos L, h\cos L + k\sin L) \tag{16}$$

1Modified Equinoctial to Cartesian

1Cartesian to Modified Equinoctial

1Keplerian to Cartesian

1Cartesian to Keplerian